

**SYNTHESIS OF ZINC SELENIDE COATED BY ZINC SULFIDE
NANOPARTICLES VIA MODIFIED POLYOL METHOD**

by

LEE SEE YAU

**Thesis submitted in fulfillment of the requirements
for the degree of
Masters of Science**

July 2011

ACKNOWLEDGEMENT

Foremost, I would like to express my highest appreciation to the Dean of School of Materials and Mineral Resources Engineering, Universiti Sains Malaysia, my main supervisor, Assoc. Prof. Dr. Sabar Derita Hutagalung and Co-supervisors, Assoc. Prof. Dr. Azizan bin Aziz and and Assoc. Prof. Dr. Ishak bin Mat. This thesis would not have been possible without their continuous guidance and support.

I would like to take this opportunity to express my gratitude to USM for financial support throughout USM Fellowship and Research University Postgraduate Research Grant Scheme for the financial support and funding in pursuing my masters' degree. Likewise, I would also like to extend my gratitude to the entire academic and technical staff especially Mdm. Fong Lee Lee in School of Materials and Mineral Resources Engineering, USM for their continuous support and patience.

My sincere thanks also go to the post graduates Khe Cheng Seong, Warapong Kengwirat and Sam Sung Ting who provide me the guidance and assistance throughout my research program. I owe my deepest gratitude to Boon Moon See, Jeremy Koh Chee Hao and Tan Wee Ching who has made available their support in a number of ways.

Finally, thousand thanks to my parents, family members, and all PTA members who had giving unconditional support and sharing during my masters' study.

LIST OF CONTENTS

	Pages
ACKNOWLEDGEMENT	ii
LIST OF CONTENTS	iii
LIST OF TABLES	ix
LIST OF FIGURES	x
LIST OF ABBREVIATIONS	xv
LIST OF SYMBOLS	xvii
ABSTRAK	xviii
ABSTRACT	xix
CHAPTER 1: INTRODUCTION	
1.1 Background	1
1.2 Problem Statement	5
1.3 Objectives	6
1.4 Project Overview	7
CHAPTER 2: LITERATURE REVIEW	
2.1 Introduction to Nanotechnology	8
2.2 Nanomaterial	9

2.3 Nanoparticles	10
2.4 ZnSe Nanoparticles	12
2.5 ZnS Nanoparticles	13
2.6 Core-Shell Structure	13
2.7 Method For the Preparation of Nanomaterials	17
2.8 Nucleation and Particle Growth Theory	19
2.8.1 Nucleation	19
2.8.2 Growth	21
2.8.3 Van der Waals Attraction Potential	23
2.8.4 Inhibition of the Agglomeration of the Nanoparticles	24
2.9 Synthesis Methods to Produce Nanoparticles	27
2.9.1 Sol-gel Process	27
2.9.2 Micelles and Microemulsions Technique	27
2.9.3 Hydrothermal Synthesis	28
2.9.4 Organometallic Route	29
2.9.5 Polyol Process	31
2.10 Tailoring the Particle Size of Nanoparticles	33
2.10.1 Effect of the Processing Temperature	33
2.10.2 Effect of Surfactant	33
2.10.3 Effect of Precursor Concentration	36
2.10.4 Effect of the Amount of Surfactant	37

2.11 Synthesis of Core-Shell Nanoparticles	37
2.12 Properties of Semiconductor Nanoparticles	40
2.12.1 Optical Properties	40
2.12.2 Non-Radiative Recombination	43
2.13 Nanoparticles Applications	44
2.13.1 Bioimaging	44
2.13.2 Light Emitting Diode	45
2.13.3 Other Applications	46

CHAPTER 3: MATERIALS AND METHODOLOGY

3.1 Introduction	47
3.2 Raw Materials	49
3.3 Synthesis of ZnSe Nanoparticles	50
3.3.1 Preparation of the Precursor	51
3.3.2 Mixing of the Precursor	52
3.4 Synthesis Parameters to Produce ZnSe Nanoparticles	53
3.4.1 Effect of Processing Time On the Formation of ZnSe Nanoparticles	53
3.4.2 Effect of the Precursor Ratio On the Formation of ZnSe Nanoparticles	53
3.4.3 Effect of the Processing Temperature On the Formation of ZnSe Nanoparticles	54

3.4.4 Effect of PEG Concentration On the Formation of ZnSe Nanoparticles	55
3.4.5 Effect of Surfactant Molecular Weight On the Formation of ZnSe Nanoparticles	56
3.4.6 Effect of Different Types of Surfactant On the Formation of ZnSe Nanoparticles	57
3.5 Synthesis of ZnSe@ZnS Core-Shell nanoparticles	57
3.5.1 Preparation of the Reactant Solution	58
3.5.2 Coating of ZnS Shell On the ZnSe Nanoparticles	58
3.6 Washing, Drying, and Storage of ZnSe Nanoparticles	59
3.7 Characterization of ZnSe Nanoparticles	59
3.7.1 Morphological and Structural Analysis	60
3.7.1.1 Field-Emission Scanning Electron Microscope (FE-SEM)	60
3.7.1.2 Transmission Electron Microscopy (TEM)	61
3.7.1.3 Phase Analysis and Crystallite Size Determination	61
3.7.2 Optical Properties Measurement	62
3.7.3 Chemical Analysis	63
3.7.3.1 Energy Dispersive X-ray Diffraction (EDX)	63
3.7.3.2 Electron Spectroscopic Imaging (ESI)	64

CHAPTER 4: RESULTS AND DISCUSSION

4.1 Introduction	65
4.2 ZnSe Nanoparticles	65
4.2.1 Effect of Processing on the Formation of ZnSe Nanoparticles	66
4.2.2 Effect of the Precursor Ratio On the Formation of ZnSe Nanoparticles	75
4.2.3 Effect of Processing Temperature on the Formation of ZnSe Nanoparticles	82
4.2.4 Effect of PEG Concentration On the Formation of ZnSe Nanoparticles	90
4.2.5 Effect of Molecular Weight and Different Type of Surfactant on the Formation of ZnSe Nanoparticles	98
4.3 ZnSe@ZnS Core-Shell Nanoparticles	108
4.3.1 Optical Analysis	108
4.3.2 Structural Analysis	111

CHAPTER 5: CONCLUSION AND RECOMMENDATION

5.1 Conclusions	119
5.2 Recommendations for Future Work	120
REFERENCES	121

APPENDICES

Appendix A

Appendix B

Appendix C

Appendix D

LIST OF TABLES

Table 3.1:	Raw Materials.	49
Table 3.2:	The effect of processing time on the synthesis of ZnSe nanoparticles	53
Table 3.3:	The effect of precursor ratio on the synthesis of ZnSe nanoparticles.	54
Table 3.4:	The effect of processing temperature on the synthesis of ZnSe nanoparticles.	55
Table 3.5:	Variation of amount of PEG that was studied.	55
Table 3.6:	Variation of surfactant molecular weight (Mw) that was studied.	56
Table 4.1:	Calculated particle size distribution, mean particle size, crystallite size, and standard deviation of ZnSe nanoparticles prepared under different processing time.	67
Table 4.2:	Calculated standard deviation, mean particle size, and particle size distribution of ZnSe nanoparticles prepared under different Zn to Se ions ratio.	80
Table 4.3:	Calculated particle size distribution, mean particle size and standard deviation of ZnSe nanoparticles prepared under different processing temperature.	87
Table 4.4:	Calculated particle size distribution, mean particle size and standard deviation of ZnSe nanoparticles prepared under different PEG concentration.	93
Table 4.5:	Particle size distribution, mean particle size and standard deviation of the ZnSe nanoparticles prepared with different molecular weight of surfactant.	102
Table 4.6:	Summary of the optimized parameters for ZnSe nanoparticles synthesis.	108
Table 4.7:	Calculated particle size range, mean particle size and standard deviation of ZnSe cores and ZnSe@ZnS core-shell nanoparticles.	115

LIST OF FIGURES

Figure 2.1:	TEM images of (a) silver nanowire (Xu et al., 2006), (b) carbon nanotube (Kwok & Chiu, 2005).	10
Figure 2.2:	TEM images of (a) Gold nanoparticles (Nakamoto et al., 2005), (b) CdSe@ZnS core-shell nanoparticles (Hines, & Guyot-Sionnest, 1996).	10
Figure 2.3:	Model of ZnSe core and ZnSe@ZnS core-shell structure.	13
Figure 2.4:	The top-down, intermediate, and bottom-up approaches to make bulk nanstructured solids (Ashby et. al., 2009).	17
Figure 2.5:	Illustration of the overall free energy ΔG as a function of the growth particle size, r (Blackman and Binns, 2009).	21
Figure 2.6:	Pair of particles used to derive the van der Waals interaction (Cao, 2004).	24
Figure 2.7:	Schematic representation of the hot injection technique employed in the organometallic synthesis of nanocrystals. (Caruso, 2004).	30
Figure 2.8:	TEM images of samples: (a) Ni nanoparticles without PVP (polyvinylpyrrolidone) (b) Ni nanoparticles with PVP (Cuoto et al., 2007).	35
Figure 2.9:	Particle morphologies obtained at 90°C for 3 hours by different cation concentration, a) 0.02M and b) 0.05M (Wang et.al, 2003).	36
Figure 2.10:	TEM images of (a) CdSe core and (b) CdSe@ZnS (Rogach,2008). (c) ZnSe core and (d) ZnSe@ZnS core-shell QDs (Fang et al., 2009).	39

Figure 2.11:	(a) Energy state of a bulk semiconductor material, (b) emission of a photon upon recombination of an electron-hole pair, (c) energy levels of an exciton. The binding energy E_B of an exciton is equal to the difference between the energy required to create a free electron and free hole and the energy to create an exciton (Ashby, 2009).	41
Figure 2.12:	(a) Absorption spectra of ZnSe nanocrystals sizes increase from the bottom to the top spectrum. (b) Photoluminescence spectra of the same series of ZnSe nanocrystals, excited with the 335nm line of an UV (Reiss et al., 2004).	42
Figure 2.13:	Trap site non-radiative recombination mechanism (Arregui, 2009).	43
Figure 2.14:	A dual-color image of QD 605-labeled <i>C. parvum</i> and QD 565-labeled <i>G.lamblia</i> (Arregui, 2009).	45
Figure 3.1:	Flowchart of the synthesis of ZnSe nanoparticles.	50
Figure 3.2:	Schematic of the setup to synthesis ZnSe nanoparticles	52
Figure 3.3:	Flowchart of the synthesis of ZnSe@ZnS core-shell nanoparticles.	58
Figure 4.1:	The illustration on formation of ZnSe nanoparticles (Gong et al., 2008).	66
Figure 4.2:	TEM image shows particle size and degree of dispersion of (a) sample T2, (b) sample T10, (c) sample T30, and (d) sample T60.	68
Figure 4.3:	Schematic diagram of the formation processes of the ZnSe nanosphere (Zhong et al., 2009).	69

Figure 4.4:	Particle size distribution of (a) sample T2, (b) sample T10, and (c) sample T30.	70
Figure 4.5:	Graph of mean particle size vs. processing time.	72
Figure 4.6:	Absorption spectra of samples prepared under different processing times.	73
Figure 4.7:	X-ray diffraction patterns for ZnSe nanoparticles prepared under different processing times: (a) sample T2, (b) sample T10, (c) sample T30, and (d) sample T60.	74
Figure 4.8:	TEM image showing the particle size and degree of agglomeration of (a) sample P1, (b) sample P2, (c) sample P3, and (d) sample P4.	76
Figure 4.9:	Particle size distributions of (a) sample P1, (b) sample P2, (c) sample P3, and (d) sample P4.	78
Figure 4.10:	Graph of mean particle size vs. the mole ratio of Zn ions to Se ions.	80
Figure 4.11:	Absorption spectra of samples with different mole ratios of Zn ions to Se ions.	81
Figure 4.12:	TEM images show particle size and degree of agglomeration for (a) sample T150, (b) sample T165, (c) sample T170, and (d) sample T195).	83
Figure 4.13:	Effect of processing temperature on the particle size distribution of (a) sample T150, (b) sample T165, (c) sample T180, and (d) sample 195.	85
Figure 4.14:	Graph of mean particle size vs. processing temperature.	88

Figure 4.15:	Absorption spectra of samples prepared with different processing temperatures.	89
Figure 4.16:	TEM image shows the particle size and degree of agglomeration of (a) sample A1, (b) sample A2, (c) sample A3, and (d) sample A4.	91
Figure 4.17:	Particle size distribution of (a) sample A1, (b) sample A2, (c) sample A3 and (d) sample A4.	92
Figure 4.18:	SEM images of samples (a) A1, (b) A2, (c) A3, and (d) A4.	94
Figure 4.19:	(a) SEM image of sample A2, which was selected for EDX testing. (b) EDX result for sample A2, which yielded carbon (C) at 19.97 at%, oxygen (O) at 22.22 at%, Zinc (Zn) at 30.14 ay%, and Selenium (Se) at 27.67 at%.	95
Figure 4.20:	Graph of mean particle size vs. concentration of surfactant.	96
Figure 4.21:	Absorption spectra of samples prepared under different surfactant concentrations.	97
Figure 4.22:	TEM images of the as-synthesised nanoparticles using different molecular weights of surfactant. Samples (a) W1, (b) W2, (c) W 3, and (d) W4.	100
Figure 4.23:	Schematic diagram of the formation of ZnSe nanoparticles without a surfactant.	103
Figure 4.24:	Schematic diagram of the formation of ZnSe nanoparticles with a surfactant.	104
Figure 4.25:	Particle size distribution of ZnSe nanoparticles prepared with different molecular weight of surfactant. (a) W1, (b) W2, (c) W3, and (d) W4.	105

Figure 4.26:	Graph of mean particle size vs. molecular weight.	106
Figure 4.27:	UV-Vis result of ZnSe nanoparticles prepared under different molecular weights of surfactant.	107
Figure 4.28:	Room temperature PL emission spectra of ZnSe core and ZnSe@ZnS core-shell nanoparticles.	109
Figure 4.29:	Room temperature optical absorption spectra of ZnSe core and ZnSe@ZnS core-shell nanoparticles.	111
Figure 4.30:	XRD pattern of (a) ZnSe and (b) ZnSe@ZnS core-shell nanoparticles.	112
Figure 4.31:	TEM images of (a) ZnSe nanoparticles and (b) ZnSe nanoparticles at higher magnification, (c) ZnSe@ZnS core-shell nanoparticle, (d) ZnSe@ZnS core-shell nanoparticle at higher magnification.	113
Figure 4.32:	Particle size distribution of (a) ZnSe core nanoparticles and (b) ZnSe@ZnS core-shell nanoparticles.	115
Figure 4.33:	ESI image of ZnSe@ZnS nanoparticles. (a) ZnSe@ZnS nanoparticles without mapping, (b) ZnSe@ZnS nanoparticles with Zn mapping, (c) ZnSe@ZnS nanoparticles with Se mapping and (d) ZnSe@ZnS nanoparticles with S mapping.	116
Figure 4.34:	Particle size distribution of ZnSe@ZnS.	118

LIST OF ABBREVIATIONS

PEG	Polyethylene Glycol
Mw	Molecular Weight
TEM	Transmission Electron Microscopy
SEM	Scanning Electron Microscopy
XRD	X-ray Diffraction
EDX	Energy Dispersive X-ray Spectroscopy
ESI	Electron Spectroscopic Imaging
PL	Photoluminescence
UV-Vis	Ultraviolet-Visible
UV	Ultraviolet
HOMO	Highest Occupied Molecular Orbital
LUMO	Lowest Unoccupied Molecular Orbital
E _g	Band gap Energy
QD	Quantum Dot
NIR	Near Infrared
PVP	Polyvinylpyrrolidone
EG	Ethylene Glycol
NP	Nanoparticle
CMC	Critical Micelle Concentration
HDA	Hexadecylamine
TOP	Trioctylphosphine
TOPO	Trioctylphosphine Oxide
Q.Y.	Quantum Yield
0-D	Zero Dimension
3-D	Three Dimensions

LCD	Liquid Crystal Display
LED	Light Emitting Diode
PVA	Polyvinyl Alcohol
FE-SEM	Field-Emission Scanning Electron Microscope

LIST OF SYMBOLS

sp^3	Hybridized orbital
ΔG	Free Energy
V	Molecular Volume
r	Radius of the Nuclei
K_B	Boltzmann Constant
S	Saturation Ratio
T	Absolute Temperature
γ	Surface Free Energy Per Unit Surface Area
r^*	Critical Size
D	Distance
Φ_A	Attraction Potential
A	Hamaker Constant
$t_{1/2}$	Half Time For Aggregation
N_∞	Number of Nuclei Formed At $t=0$
μ	Viscosity
λ	Wavelength
D	Crystallite Size
β	Full Width at Half Maximum
θ	Position of the Peak

SINTESIS NANOPARTIKEL ZINK SELENIDA DISALUT DENGAN ZINK SULFIDA MELALUI KAEDAH POLIOL TERUBAHSUAI

ABSTRAK

Nanopartikel Zink Selenida (ZnSe) dan struktur kelompang teras Zink Selenida@Zink Sulfida (ZnSe@ZnS) telah dihasilkan melalui kaedah poliol terubahsuai. Nanopartikel ZnSe dihasilkan dengan menggunakan Zink Klorida dan serbuk selenida sebagai bahan pemula. Nanopartikel ZnSe yang dihasilkan akan disalut dengan ZnS untuk menghasilkan struktur kelompang teras ZnSe@ZnS. Objektif kajian ini adalah untuk menghasilkan nanopartikel yang bersaiz kecil dan mempunyai taburan saiz yang sempit dengan mengubah pelbagai parameter. Parameter-parameter yang dikaji termasuk jangka masa pemrosesan, nisbah bahan permula, kepekatan surfaktan, jisim molekul serta jenis surfaktan yang berbeza. Keadaan optimum untuk menghasilkan nanopartikel ZnSe yang bersaiz kecil serta mempunyai taburan saiz yang sempit adalah pada suhu 195°C dengan masa pemrosesan selama 2 minit. Nisbah bahan pemula Zn kepada Se yang sesuai adalah 1:1. 0.02g surfaktan PEG yang berjisim molekul 10,000 didapati adalah paling sesuai dalam menghasilkan nanopartikel ZnSe yang bersaiz purata 2.96 nm dan taburan saiz dalam lingkungan 1.5-4.5 nm. Analisis menggunakan TEM dan SEM telah mengesahkan bahawa nanopartikel ZnSe dan struktur kelompang teras ZnSe@ZnS yang dihasilkan adalah bersaiz kecil, berbentuk separa bulat dan mempunyai pengaglomeratan sederhana. Penghasilan nanopartikel ZnSe dan ZnSe@ZnS dengan berjaya telah dibuktikan dengan ujian XRD, EDX dan ESI. Keputusan ujian PL menunjukkan bahawa puncak pemancaran pada 402 nm manakala UV-Vis menunjukkan puncak penyerapan pada 464 nm. Penyalutan ZnS ke atas permukaan nanopartikel ZnSe telah berjaya dan dibuktikan oleh peningkatan keamatan PL yang drastik serta anjakan merah oleh ujian UV-Vis.

SYNTHESIS OF NANOPARTICLES OF ZINC SELENIDE COATED BY ZINC SULFIDE VIA MODIFIED POLYOL METHOD

ABSTRACT

Zinc selenide (ZnSe) nanoparticles and zinc selenide@zinc sulphide (ZnSe@ZnS) core-shell structure were prepared using a surfactant-assisted process. ZnSe nanoparticles were prepared using zinc chloride and selenium powder as the precursor sources. The obtained ZnSe nanoparticles were then coated with ZnS to form the ZnSe@ZnS core-shell structure. Various parameters namely processing time, processing temperature, precursor ratio, concentration of surfactant, molecular weight of surfactant, and type of surfactant have been studied in order to produce finer particle with narrow particle size distribution of the ZnSe and ZnSe@ZnS core-shell nanoparticles. The optimum condition for the synthesis of ZnSe nanoparticles was 195°C for 2 minutes with the Zn to Se ions ratio of 1:1. Furthermore, 0.02g of 10,000 Mw polyethylene glycol (PEG) was found to be the most effective surfactant to form the nanoparticles with the mean diameter of 2.96 nm and particle size distribution within 1.5 – 4.5 nm. TEM and SEM analysis confirmed that the synthesized ZnSe and ZnSe@ZnS core-shell nanoparticles had a small particle size and a quasi-spherical shape with mild agglomeration. The success for the formation of ZnSe and ZnSe@ZnS core-shell nanoparticles was further confirmed by XRD, EDX, and ESI testing. PL and UV-Vis analysis recorded emission and absorption wavelength at 402 nm and 464 nm respectively. The successful of ZnS coating on ZnSe cores were confirmed by the drastic enhancement of PL intensity and red shift of ZnSe@ZnS absorption peak from UV-Vis testing.

CHAPTER 1

INTRODUCTION

1.1 Background

Generally, nanotechnology is defined as the systematic manipulation, alteration of structures, systems, materials, or components in the range of atomic or molecular dimensions from 1 to 100 nm (Sepeur et al., 2008). A nanoparticle is outlined as a particle within the size range of 1 to 100 nanometers (Sergeev, 2001). Nanoparticles are important due to their unique properties when at the nanoscale level. When a material is at a macroscopic level, it should always display constant physical properties regardless of the size. Nevertheless, when the material is at the nano-scale, its properties are altered. For a semiconductor, this can be explained by the confinement effect of the electronic motion (length scale), which is smaller at the nano scale than the electronic motion in a bulk semiconductor (Cao, 2004). Besides, the large surface to volume ratio of nanoparticles also contributed to these unique properties. Furthermore, Nikesh & Mahamuni (2001) claim that the unique properties of nano-scale particles was attributed to the discretisation energy levels, the concentration of oscillator strength for particular transitions, and the high polarisability of electron energy levels.

Therefore, the desired properties of nanoparticles can be obtained by tailoring the particle size and modifying the surface conditions of the nanoparticle (Nanavati et al., 2009). These unique size-dependant properties make it a potential candidate for various photoelectronic applications and advanced biological applications, such

as their use in optoelectronic devices, LEDs, lasers, and biological labels (Andrade et al., 2008). By coating an organic layer on the nanoparticle through the formation of a chemical bond with the particle surface, the nanoparticle is useful for biological cell dissolution, magnetic separation of minerals, and elimination of toxic elements from industrial waste (Prozorov et al., 1999).

In the last decade, effort has been dedicated to the preparation of high-quality nanoparticles, and studies have focused on the adjustments of general experimental conditions, such as precursors, ligands, stabilising agents, reaction temperatures, and the addition of nucleation agents. (Cadmium selenide) CdSe (quantum dots) QDs are a very successful example due to their high emission efficiency and size-dependent photoluminescence (PL) properties. However, the limited efficient emissions in the green to near-infrared range have limit its applications (Chen et al., 2004). Apart from CdSe, CdTe, CdS, and alloy nanocrystals are other examples of high-quality nanoparticles that have been successfully synthesised via organometallic or aqueous approaches (Fang et al., 2009).

The intrinsic toxicity of cadmium has been reported by Xing et al. (2008) and Li et al. (2004). This disadvantage has limit its potential for its applications. Hence, researchers have looked for a better candidate to replace the cadmium base semiconductor. ZnSe has been noted as a better option because of its lower toxicity, and it is more environmentally friendly compared to other wide band gap materials (Fang et al, 2009). The band gap energy of ZnSe is 2.7 eV, which is better than CdSe because it is able to offer intense UV blue luminescent properties that cannot be achieved using CdSe (Hwang and Cho, 2005). Agglomeration and particle size are

general problems with the synthesis of nanoparticles. Thus, many efforts have been made to develop a better synthetic method of producing the colloidal ZnSe nanoparticles with a controlled size and size distribution (Lomascolo et al., 2003). For example, the wet chemical route is able to synthesise nanoparticles at a lower temperature, while the reverse micelle method is able to prepare nanoparticles with 3-4 nm particle size range.

The surface area of the particle will increase when the size of the particle decreases. The high surface to volume ratio of the particle plays a vital role in deciding the particle's electronic and optical properties (Amit et al., 2007). This is due to the large amount of atoms that are localized on the surface of the nanocrystals. Thus, extensive research has been conducted on the surface chemistry of the semiconductor nanoparticles. It was proposed by Koberling et al. (1999) that the presence of defects on the particle surface has potential to degrade the optical properties of the nanoparticles and results in low photoluminescence (PL) efficiency. This is due to the formation of radiation less recombination centres that occur on the nanoparticles surface (Koberling et al., 1998). According to Hwang and Cho, (2005), coating a larger inorganic band gap material on the nanoparticle can enhance the photoluminescence (PL) efficiency and stability. However, Nikesh et al. (2001) reported that the ZnSe@ZnS core-shell system yielded a remarkable enhancement of the PL quantum yields. Fang et al. (2009) also recorded a photoluminescence quantum yield (PLQY) that was 65% and strong stability after coating a monolayer of ZnS on the surface of ZnSe quantum dots. An enhancement in the localisation of charge carriers was achieved through this core-shell system. Both cationic and anionic dangling bonds were successfully passivated, and thus, the nonradiative

recombination sites were eliminated by capping the nanoparticles with a higher band gap inorganic semiconductor.

A high quality core-shell structure can be obtained via the organometallic process, which involves the use of toxic chemicals, such as trioctylphosphine (TOP), trioctylphosphine oxide (TOPO), hexadecylamine (HDA), and diethylzinc (ZnEt_2) (Xiong et al., 2007; Murase and Gao, 2004). Apart from the toxicity, the organometallic process requires a high processing temperature to obtain high-quality core-shell nanocrystals. This is limited by its application, cost-effectiveness, and environmental friendliness. Another point of concern is the lattice mismatch which become important when choosing the candidate for the coating of ZnSe quantum dots. Large lattice mismatches will lead to the delamination of the shell from the core and result in strains between the core and the shell. Thus, the result of imperfect coating will lead to problems such as the degradation of electronic properties, which affect the PL efficiency. Because of this, the 5% lattice mismatch of ZnS and ZnSe qualified as the best candidate for the shell of the ZnSe quantum dots (Song and Lee, 2001).

Generally, controls against agglomeration, particle size, and particle size distribution are problems faced by most researchers. Therefore, many studies have focused on how to prepare the nanoparticles with small particle size and a narrow particle size distribution. Therefore, a surfactant was introduced to improve these properties. Surfactant plays a key role in the synthesis process because they serve as a protective agent to the nanoparticles (Shi et al., 2008). According to Cao (2004), surfactant produces steric hindrance between nanoparticles by forming a thin layer

on the surface of the nanoparticles. This steric hindrance is able to inhibit the nanoparticles from agglomeration and control the particle growth (Cao, 2004). Therefore, the addition of surfactant is able to produce nanoparticles with smaller particle size (Gong et al., 2008). However, the addition of the surfactant has limitations. The surfactant tends to complicate the cleaning process of the nanoparticles. The absorbed surfactant is difficult to completely remove from the surface of the nanoparticles by centrifugation. Perhaps secondary cleaning processes, such as annealing, are needed to burn away the surfactant from the surface of the nanoparticles (Wu and Chen, 2003). Furthermore, the selection of a suitable surfactant for a particular reaction is a tedious task of trial and error. There are many matters that have to be taken into consideration when choosing a suitable surfactant. For example, the solubility of the surfactant in a solvent, the molecular weight, and the amount of the surfactant needed. Thus, in some cases, the agglomeration of nanoparticles still cannot be avoided even with the presence of a surfactant.

1.2 Problem Statement

Newly formed ZnSe nanoparticles are subject to the surface defect during the synthesis process. This surface defect will act as the trap to degrade the optical properties of the nanoparticles. Hence, surface modification has to be done to remove the defects. This can be achieved by coating a larger band gap semiconductor such as ZnS on the surface of the ZnSe nanoparticles to form a core-shell structure. This core-shell structure is believed to be possible to enhance the luminescence intensity of the nanoparticles (Chen et al., 2004). However, the feasibility of this method remains questionable.

Many synthesis methods of ZnSe and ZnSe@ZnS nanoparticles have been reported to date. Among these methods are the organometallic method, reverse micelle, micelle, solvothermal, hydrothermal, and the wet chemical route. However, all of these methods have to seriously consider the cost, toxicity, precursor availability, environmental issues, and ease of the experiment setup (Hines and Guyot Sionnest, 1996; Burda et al., 2004; Fang et al., 2009).

As reviewed, the synthesis of ZnSe@ZnS core-shell nanoparticles using an organic solvent still remains less unexplored. In this project a new method was designed to synthesize ZnSe and ZnSe/ZnS nanoparticles at much lower temperatures using Se powder as a selenium source and using ZnCl₂ as a Zn source, respectively. In contrast to the previous studies, this greener synthesis method is performed at much lower temperatures which are below 200°C, use nontoxic or low-toxic chemicals as precursors, do not use inert gas and complicated equipment.

1.3 Objectives

- 1.** To synthesize the ZnSe core nanoparticles with smallest size and narrowest size distribution via modified polyol method. This is achieved by varying different parameters to optimise the outcome.
- 2.** To synthesise the ZnSe@ZnS core-shell nanoparticles.
- 3.** To study the morphology, crystal structure, and optical properties of the ZnSe and ZnSe@ZnS core-shell nanoparticles.

1.4 Project Overview

In the present study, ZnSe and ZnSe@ZnS nanoparticles are synthesised with the assist of a surfactant. The project was divided into two major parts. The first part involved the synthesis of the ZnSe nanoparticles, and the second part involved the coating of ZnS on the ZnSe nanoparticles to form the ZnSe@ZnS core shell structure. In the first part, parameters, such as the processing time, ratio of precursors, processing temperature, effect of different concentrations of the surfactant, the effect of different molecular weights of surfactant, and the effect of different types of surfactant on the synthesis of ZnSe nanoparticles, were studied. The parameters were optimised to obtain the narrowest particle size distribution and the smallest particle size of ZnSe nanoparticles for subsequent production of the ZnSe@ZnS core shell structure in the second part.

Standard characterisation techniques, such as (scanning electron microscopy) SEM, (transmission electron microscopy) TEM, (x-ray diffraction) XRD, (electron spectroscopic imaging) ESI, (ultraviolet–visible) UV-Vis spectroscopy, and photoluminescent spectroscopy, were performed on the synthesised ZnSe and ZnSe@ZnS nanoparticles.

CHAPTER 2

LITERATURE REVIEW

2.1 Introduction to nanotechnology

Generally, nanoscience is defined as the study of phenomena within the scale from 1 to 100 nm. Nanotechnology on the other hand is about the ability to create, control and manipulate materials that in this range with the goal to produce new materials with specific properties (Blackman and Binns, 2009). Nanotechnology covers a broad field of research and interdisciplinary and multidisciplinary efforts are required. The area includes physics, chemistry, biology, engineering, medicine and materials science, and impacts on other disciplines as well (Cao, 2004).

Nanoscience is not a new thing. It was mentioned as early as 1857 by Faraday in his studies on gold particles (Laguna, 2008). The motivation for his study was from the red color of the gold particles, which shows a big contrast to the yellow appearance of gold in its bulk form that we are familiar with. Moreover, by a similar argument, the use of nano-size small metal particles in production of stained glass that are widely used in church windows or in pottery glazes decoration would date nanotechnology back to mediaeval times or even earlier (Blackman and Binns, 2009).

Nano-objects are the material that have a size that is intermediate between atoms (or molecules) and bulk matter. The properties of the nano-objects are in big contrast relative to the bulk material due to the surface properties. It is believed that

even for a clusters that have 1000 atoms; more than one-quarter of the atoms are concentrated on the surface. Therefore, the size, shape and composition of the nanoparticle is strongly related to the properties of the nanoparticles (Blackman and Binns, 2009; Mathew et al., 2007).

Recently, nanotechnology plays more important roles in both biomolecular detection and medical diagnostics fields. It provides a faster, more reliable, quantitative, lower cost and multi-channel identification for biomarkers as genes and proteins is the factor that rate-limiting step for the clinical deployment of personalized medicine (Blackman and Binns, 2009; Sharma et al., 2006). In electronic application, the density of chips on a component is able to be increased by the application of nanotechnology. The respond time of the component was shorten due to the shorter distance that has to be traveled by the electrical signal. Thus, the performance of the component becomes faster. The preparation, general properties and the factors that influence these properties are important and a well understand on these criteria can utilize the materials more effectively (Mamalis, 2007).

2.2 Nanomaterial

Nanomaterials are the materials where sizes of the individual building blocks are within the nanometer scale which is below 100 nm in at least one dimension. This definition is applicable for many research proposals, where nanomaterials deserve high priority. Nanomaterials could exist in zero-dimensional (e.g., nanoparticles), one-dimensional (e.g. nanorods or nanotubes), or two-dimensional (usually realized as thin films or stacks of thin films) (Cao, 2004).

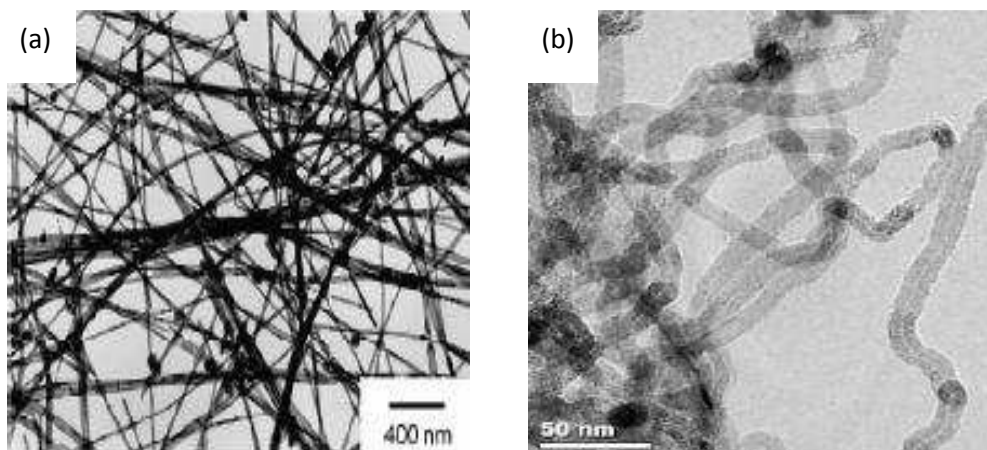


Figure 2.1: TEM images of (a) silver nanowire (Xu et al., 2006), (b) carbon nanotube (Kwok & Chiu, 2005).

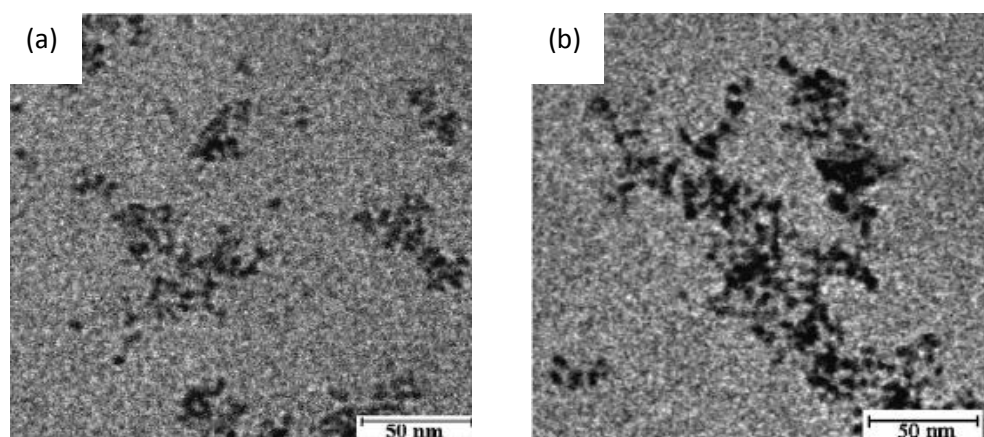


Figure 2.2: TEM images of (a) CdSe nanoparticles (b) CdSe@CdS core-shell nanoparticles (Deng et al., 2006).

2.3 Nanoparticles

A particle having one or more dimensions of the order of 100 nm or less is considered as nanoparticles. The study on how to reduce the size of bulk materials to the nanometer scale has led to an interesting class of novel materials that have characteristics between the classic bulk and molecular descriptions. Nanoparticles with radii of less than the mean distance between the electron and hole are showing quantum confinement, known as the bulk exciton Bohr radius (Song and Lee, 2001). The spherical nanocrystals electronic states can be explained by considering a

spherical particle, where the electron and the hole are limited in a small area. In this model, the electrons and holes that carried by the charge are confined by a potential that is infinite at the nanocrystal surface. Hence, nanoscopic semiconductors exhibit larger band gaps relative to the bulk material and have discrete excitable states (Skaff and Emrick, 2004).

Band gap energies of nanoscopic semiconductors are strongly dependent on its size. The radius of the nanocrystal is inversely proportional to the band gap energy, such that as the radius of the nanocrystal decreases, the band gap increases. This allows tuning the emission wavelength of the nanoparticle by adjusting the particle size within the quantum-confined regime (Skaff and Emrick, 2004).

Semiconductor nanocrystals have been reported from a variety of compositions, including CdSe (Knox et al., 2006), CdS (Wei et al., 2007), ZnSe (Lei et al., 2008), and InP (Lampert et al., 2006). Excitation of an electron from the highest occupied molecular orbital (HOMO) to the lowest unoccupied molecular orbital (LUMO) leads to the rapidly moving charge carriers. During excitation, a little lattice distortion was experienced by these sp^3 hybridized systems and thus preclude the formation of defects and allow the charge carriers to move freely through the nanocrystal. Additionally, the radiationless internal conversion or the conversion of electronic energy to heat is slower. Thus, the combination of all these factors along with the quantum confinement effect result to the good luminescence in nanoparticles that is unavailable in bulk semiconductors. However, the luminescence intensity are degraded as defects will formed during the synthesis preparation. These defects were act as a trap to capture the electron and hole and finally lead to the non-

radiative emission and thus degrade the luminescence properties (Skaff and Emrick, 2004).

2.4 ZnSe Nanoparticles

II-VI semiconductors are combination of an element from group 2 and an element from group 6 of the periodic table of elements (Reiss et al., 2004). Generally, the bandgap (E_g) of group II-VI semiconductors is constituent atoms dependent. The bandgap (E_g) of the semiconductors will become narrower when the constituent atoms become heavier. For the nanoparticles with the diameters of approximately 2-10 nm, the quantum size effect will increase the bandgap compared to the bulk semiconductor. It also will lead to various fluorescent colors reflecting small differences in the particle size (Hosokawa et al., 2007). One of the most successful examples of the II-VI semiconductors is ZnSe nanoparticles. ZnSe has bulk band gap of 2.7 eV (Balasubramanian et al., 2009). The band gap energy of 2.7 eV and emission wavelength of 460 nm is a property that is not observed in other nanocomposite like CdSe and CdS (Hwang and Cho, 2005). It is a II-VI semiconductor and show intense UV blue luminescent properties with low toxicity. Due to these unique properties, it is widely used in photoelectronic application and advanced biological applications. Hence, efforts have been made to obtain nanoparticles of ZnSe (Xing et al., 2008; Fang et al., 2009).

Semiconductor nanoparticles can have high emission yields covering the visible and near infrared (NIR) spectrum due to quantum effects. The quantum yield and emission life-time of the band gap luminescence are dependent on the condition

of the surface of the nanoparticles. It is learned that the as synthesized bare ZnSe nanoparticles tend to have many surface defects, which cause non-radiative deactivation after excitation. Also, such nanoparticles are easily agglomerated which will cause imperfect chemical bonds between nanoparticles (Cao, 2004).

2.5 ZnS Nanoparticles

Zinc sulphide is one of the II-VI semiconductors. The nanoparticles from this group is attracting much attention due to their size-dependent photo- and electro-luminescence properties like ZnSe and these unique properties offers promising applications in optoelectronics. ZnS has a wide band gap thus it is very attractive for the optoelectronic application especially in nanoscale form. ZnS is available in two crystal structure which is zinc blende and wurtzite. Besides, ZnS has a direct band structure with band gap energy of 3.68 eV (Denzler et al., 1998; Saravanan et al., 2008).

2.6 Core-shell Structure

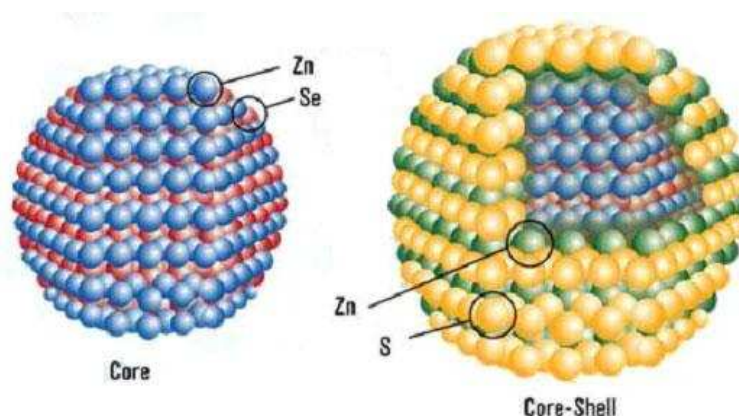


Figure 2.3: Model of ZnSe core and ZnSe@ZnS core-shell structure.

It is unavoidable that the surface of the new formed nanoparticle tends to have some lattice defects during the nanocrystal synthesis process. For example, surface atoms could miss at least one chemical bond. The consequence of these defects will dramatically reduce the fluorescence quantum yield of the QDs due to the non-radiative annihilation of the excited electron-hole pairs in these defects. However, by doing some modification on the surface of the QDs can solve this problem. It means by removing or reducing the non-radiative surface recombination sites and confine charge carriers are believed to be possible to enhance the luminescence yields of the QDs (Chen et al., 2004).

Generally there are two type of passivation method that is always employed in the QDs. The first one is through band gap engineering which is reconstructing the loose bonds to passivate the surface defects. This passivation can be achieved by coating the QD nanoparticles with a larger band gap semiconductor. A good lattice mismatch is required to obtain a good result. This topology is called core-shell structure. The second method is the adsorption of Lewis bases on the QD surface. For example, passivate the surface of CdSe and CdSe/ZnS quantum dots with otylamine is the best to describe this method. In this project, focus will fall on the first method which is passivation through band gap engineering (Cao, 2004). In a core-shell QDs, the shell semiconductors play two simultaneous roles. The first role is passivate the surface traps of the core and the second one is to act as a protective layer against external aggressive agents (Arregui, 2009). Due to this ability to protect the active core against external aggressive agents, so the core-shell configuration is more robust to photobleaching, pH changes, or other potentially aggressive media.

There are numerous reports of core-shell quantum dots that worth to refer to and some examples are ZnS (shell) on CdSe (quantum dots) (Sambur and Parkinson, 2009; Dabbousi et al., 1997), CdS on CdSe (Wang et al., 2006; Cherniavskaya et al., 2003), ZnS on InP (Ryu et al., 2009), ZnCdSe₂ on InP (Micic et al., 2000) and there are not much research is done on ZnSe@ZnS (Figure 2.3). There are several aspect have to take into consideration when choosing the correct shell material for the QDs so that the semiconductor shell permits the light emitted from the core quantum dot does not absorbed by the shell layer. Wider bandgap semiconductor with a small lattice mismatch with the core semiconductor is suitable to form core-shell structure.

Referring to Prasad (2004), there are many interesting finding from the formation of CdSe-ZnS core-shell quantum dots. One of them is a small red shift in the adsorption spectra of the CdSe-ZnS core-shell quantum dots compared to the bare CdSe. This small red shift is due to the partial leakage of the electronic wave function into the shell semiconductor. When ZnS is coated on the CdSe core, the wave function of the electron is spread into the shell but the wave function of the hole is remains localize in the CdSe core. This effect causing the bandgap getting narrower thus leading to the red shift of the adsorption. The difference between the bandgaps of the core and the shell semiconductor will influence the red shift phenomena. The red shift becomes smaller as the difference between the bandgaps increases. In addition, the red shift is more obvious for a smaller size quantum dot where the spread of the electronic wave function to the shell structure is increased. When the ZnS shell layer is increased for the same size CdSe quantum dot (~4nm), an increase red shift of emission peak compared to the absorption peak is observed through photoluminescence spectra, with an increase in broadening of the peak. The

reason behind this effect is mostly due to the inhomogeneous distribution of the size and preferential absorption into larger dots (Prasad, 2004).

The shell layers of the core-shell QDs play an important role in define the luminescence quality of the QDs. So, there are some aspects have to take into consideration when growing the shell semiconductor on a core semiconductor. Among them are growing temperature and concentration of the growth species. Homogeneous nucleation must be avoided when growing a layer of larger band gap semiconductor on the surface of a nanoparticle. To achieve heterogeneous nucleation, supersaturation should not too high for nucleation but high enough for growth. This can be done by controlling the concentration of the growth species.

There are two methods can be applied to control the supersaturation of the growth species. The first one is by adding the growth precursor into the reaction mixture which contains the cores nanoparticles drop wise. The second method is by varying the growth temperature. Lower temperature can produce smaller nanoparticles (Hwang and Cho, 2005). It was mentioned earlier that both anionic and cationic surface dangling bonds can be eliminated by growing the shell semiconductor on a core nanoparticle. For example, the wurtzite CdSe-CdS core-shell nanoparticle is ideal in many aspects. The small lattice mismatch of 3.9 % between CdSe and CdS is small enough to allow heteroepitaxial growth, and large enough to prevent alloying. Besides, the difference in bandgaps is large enough for shell growth to enhance the quantum yield and the stability of the cores. For the synthesis of CdSe/ZnS core/shell nanostructures, the temperatures and size for each CdSe core was coated are as follows: 140°C for 2.3 and 3.0 nm diameters, 160°C for

3.5 nm, 180°C for 4.0 nm, 200°C for 4.8 nm, and 220°C for 5.5 nm. The particle size is dependent on the synthesis temperature and thus the temperature for the growth on smaller nanoparticles is lower (Cao, 2004).

2.7 Method for the preparation of nanomaterials

Figure 2.4 illustrates the top-down, intermediate, and bottom-up approaches to prepare bulk nanostructured solids. Generally, top-down and bottom-up routes are two major approaches for the synthesis of nanomaterials and the nanostructures fabrication. Milling is a typical top-down method in making nanoparticles, whereas the colloidal dispersion is a good example of bottom-up approach in the synthesis of nanoparticles. Lithography is so unique and it can be considered as a combination of both top down and bottom up approaches. This is because of the growth of thin films is categorized as bottom-up whereas etching is top-down approach, while nanolithography and nanomanipulation are commonly referred as a bottom-up approach. In modern industry, both approaches play a very important role and most likely in nanotechnology as well.

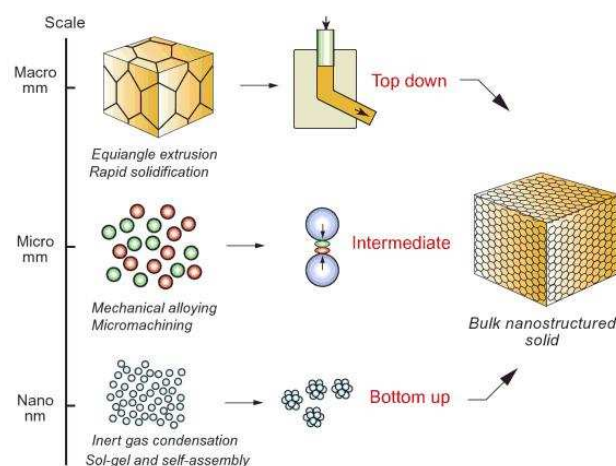


Figure 2.4: The top-down, intermediate, and bottom-up approaches to make bulk nanostructured solids (Ashby et. al., 2009).

There are advantages and disadvantages in both approaches, imperfection of the surface structure is the biggest problem that is faced in top-down approach. In top-down techniques, two of the common problems are the damage of crystallographic structure to the processed patterns in lithography and additional defects that are introduced during etching process. For example, in the nanowires fabrication, the nanowires that are produced using lithography method contain a lot of impurities and structural defects on their surface. In addition, the surface was rough. This surface defects cause low conductivity which is caused by the inelastic surface scattering. As a result from these phenomena, excessive heat will be generated and thus increase the difficulties to the device design and fabrication. Top-down approach will continue to play an important role in the nanostructures and nanomaterials fabrication even though it will lead to surface imperfection and other defects (Pallab, 2009).

Bottom-up approach is nothing new in materials synthesis but it is still often emphasized in nanotechnology literature. Typical material synthesis is to build atom by atom on a very large scale, and has been widely used in industries for a long time. For examples, the production of salt and nitrate in chemical industry, the growth of single crystals and films deposition in electronic industry. The chemical composition, crystallinity, and microstructure of a material are highly influenced by the synthesis approaches due to the kinetic reasons. Hence, the material will exhibits difference physical properties (Cao, 2004; Joshi, 2008).

Generally, bottom-up approach always refers to build-up material from bottom like building from atom by atom, molecule by molecule, or cluster by cluster.

In organic chemistry, polymer is synthesized by linking the individual monomers together. Growth species like atoms, ions and molecules are assemble into crystal structure from one after another after impinging onto the growth surface during crystal growth. Top-down approach has its limit on synthesis nanometer materials. The tools that possessed are too big to deal with such tiny subjects. Thus, the bottom-up approach reserves an important place in the fabrication and processing of nanostructures and nanomaterials (Cao, 2004; Koch, 2003).

When put top-down approach and bottom-up approach under comparison, the latter one provide a better chance to obtain nanostructures with better quality. These including less defects, more homogeneous chemical composition, and better short and long range ordering. The reason for these advantages are due to the bottom-up approach is driven mainly by the reduction of Gibbs free energy, thus the nanostructures and nanomaterials produced more thermodynamic equilibrium. In contrary, top-down approach will introduce internal stress, surface defects and contaminations in the nanomaterial produced (Cao, 2004; Gabriel, 2004).

2.8 Nucleation and particle growth theory

2.8.1 Nucleation

The chemical growth of bulk or nanometer-sized material is precipitated of a solid phase from solution. By well understand the process and parameters that control the precipitation helps to improve the engineering of the growth of nanoparticles to the desired size and shape. For a particular solvent, there must be

certain solubility for a solute, whereby addition of any excess solute beyond the solubility level of the solute will result in precipitation and formation of nanocrystals. Hence, for nucleation to occur in nanoparticle, the solution must be supersaturated. This can be achieved either by directly dissolving the solute at elevated temperature and then cooling to low temperatures or by adding the required reactants to form a supersaturated solution during the reaction. The precipitation process basically consists of two steps which are nucleation and particle growth stages (Wang et. al., 2003). Generally, the nucleation processes can be divided as follow: homogeneous nucleation, heterogeneous nucleation, and secondary nucleation. Homogeneous nucleation occurs without a solid interface by combining solute molecules to produce nuclei. Homogeneous nucleation is initiated by the driving force of the thermodynamics because of the supersaturated solution is not stable in ΔG , overall free energy (Wang et al., 2003; Sugimoto, 2001).

$$\Delta G = -\frac{4}{V}\pi r^3 k_B T \ln(S) + 4\pi r^2 \gamma \quad (2.1)$$

where V is the molecular volume of the precipitated species, r is the radius of the nuclei, k_B is the Boltzmann constant, T is the temperature, S is the saturation ratio, and γ is the surface free energy per unit surface area. When $S > 1$, ΔG has a positive maximum at a critical size, r^* as shown in Figure 2.5. This maximum free energy is the activation energy required for nucleation to happen. The free energy will decrease for the nuclei larger than the critical size. This reduction in free energy is needed for the growth and form stable nuclei that grow to form particles. The critical nuclei size r^* can be obtained by setting $d\Delta G/dr = 0$

$$r^* = \frac{2V\gamma}{3k_B T \ln(S)} \quad (2.2)$$

For a given value of S , all particles with $r > r^*$ will grow and all particles with $r < r^*$ will decomposed. From the Equation (2.2), the critical nuclei size, r^* is inversely proportional to the saturation ratio S (Wang et. al., 2003).

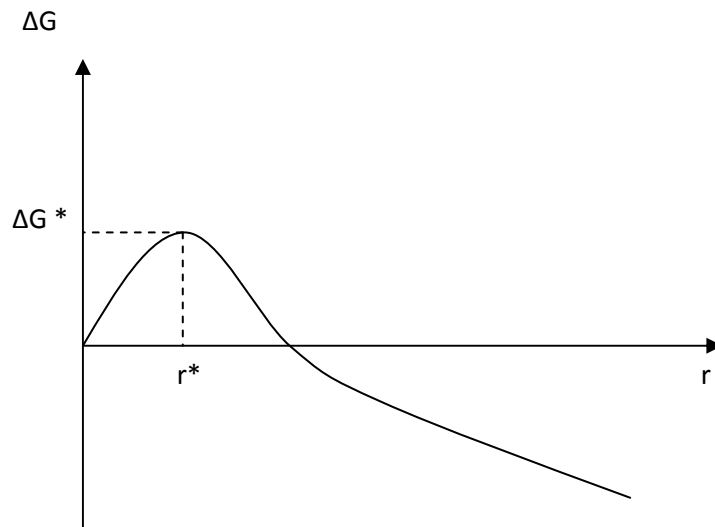


Figure 2.5: Illustration of the overall free energy ΔG as a function of the growth particle size, r (Blackman and Binns, 2009).

2.8.2 Growth

After the nuclei are successfully formed from the solution, they grow by deposit the soluble species onto the solid surface. This is termed as molecular addition. When the concentration falls below the critical level, nucleation will stops. At the same time, the particles will continue to grow by the molecular addition process until the concentration of the species is equilibrium. The growth rate for the smaller particle was faster than larger particles at this stage. This can be explained by assuming the larger ones are slightly bigger than the critical size, thus the free energy

that driving the growth is larger for the smaller particles. A nearly monodisperse size distribution can be obtained if the nucleation and growth is terminated quickly. Beside this method, an alternative strategy to obtain monodisperse distribution is by repeated injections of the metal precursor(s) to maintain a saturated condition throughout the reaction (Blackman and Binns, 2009; Burda et al., 2005).

When the particle growth, the reactants are depleted. This will lead to the different growth rate of small and large particles. In this case, Ostwald ripening will occur. The saturation ratio (S) is decreasing and the corresponding critical nuclei size (r^*) is increasing (Equation (2.2)). Particles that are smaller than this new critical size will continue to shrink and finally disintegrate, while the larger one will continue to grow. A broad size distribution of particles will happen if stop the reaction at this point. If the reaction is allowed to continue until the supersaturation is depleted, the smaller nuclei will vanished completely and form to monodispersed particles with relative large particle (micrometer-size) (Blackman and Binns, 2009; Burda et al., 2005).

Another factor that has to be considered is secondary growth which is the growth of particles by aggregation with other particles. Growth by this process occurs by stable particles combining with smaller unstable nuclei. The growth by secondary growth is faster than that by molecular addition (Blackman and Binns, 2009). Finally, it should note that nanoparticles are small and are not thermodynamically stable. Therefore it is necessary to stabilize them either by adding surface-protecting reagents, such as organic ligands or inorganic capping materials, or by placing them in an inert environment, such as an inorganic matrix or

polymer. A suitable choice of capping material is important to provide a barrier to counteract the attraction between nanoparticles due to the van der Waals attraction (or magnetic attraction in the case of magnetic materials) (Blackman and Binns, 2009; Wang et al., 2003).

2.8.3 Van der Waals attraction potential

When particles are small, typically below micrometers, and are dispersed in a solvent, van der Waals attraction force and Brownian motion play important roles. Van der Waals force is a weak force. It becomes significant when at a very short distance. Brownian motion ensures that the collision of nanoparticles with each other happen all the time. The combination of these two effects would lead to the formation of agglomeration of the nanoparticles (Cao, 2004; Koch, 2003).

Van der Waals interaction between two nanoparticles is the sum of the molecular interaction for all pairs of molecules composed of one molecule in each particle, as well as to all pairs of molecules with one molecule in a particle and one in the surrounding medium such as solvent. Integration of all the van der Waals interactions between two molecules over two spherical particles of radius, r , separated by a distance, D , as illustrated in Figure 2.6 gives the total interaction energy or attraction potential:

$$\Phi_A = -\frac{A}{6} \left\{ \frac{2r^2}{D^2+4rD} + \frac{2r^2}{D^2+4rD+4r^2} + \ln \left(\frac{D+4rD}{D^2+4rD+4r^2} \right) \right\} \quad (2.3)$$

Where the attraction nature of the interaction between two particles are denoted by the negative sign, and A is a positive constant termed the Hamaker constant which has a magnitude on the order of 10^{-19} to 10^{-20} J and depends on the polarization properties of the molecules in the two particles and in the medium which separates them.

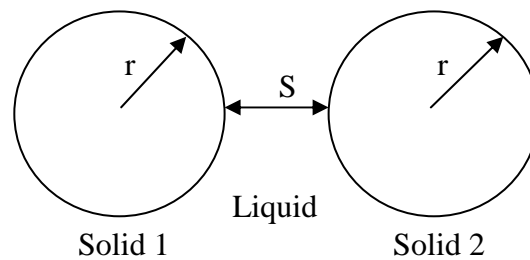


Figure 2.6: Pair of particles used to derive the van der Waals interaction (Cao, 2004).

The attraction force between two particles is inevitable have to be overcome from agglomeration. As a result, developing a barrier potential between two particles are believed able to prevent agglomeration. There are two methods are widely applied to prevent agglomeration of particles which is electrostatic repulsion and steric exclusion (Cao, 2004; Chow and Gonsalves, 1996).

2.8.4 Inhibition of the agglomeration of the nanoparticles

Smaller particles will have higher surface energy and thermodynamically unstable. Thus, nanoscale particles always minimize the total surface or interfacial energy of the system by agglomerate to form either lumps or secondary particles. When the particles are strongly stuck together, these hard agglomerates are called aggregates. Agglomeration of small particles can occur at various stages including synthesis stage, drying stage and subsequent processing of the particles. Thus

stabilize the particles from adverse agglomeration at each step of particle production is very important and needed. Stabilizing agent of surfactants is used to stabilize the particles in the synthesis process or disperse as-synthesized agglomerated fine particles (Astruc, 2008).

As discussed earlier, fine particles have larger surface energy and are thermodynamically unstable. Thus, to become stable, they tend to minimize the total surface energy of the system by agglomeration. Agglomeration happens with the assistance of the attractive van der Waals force. Therefore, interparticle repulsive forces are required to prevent the agglomeration of these particles. Commonly, there are two methods used to prevent the agglomeration of nanoparticles. There are electrostatic stabilization and steric stabilization (Chow and Gonsalves, 1996). Electrostatic stabilization provides dispersion by producing electrostatic repulsion. The repulsion force arises from the interactions between the electric double layers surrounding the particles. There is always an unbalanced charge distribution always exists between a particle surface and the solvent. Electrostatic stabilization of dispersion occurs when the electrostatic repulsive force overcomes the attractive van der Waals forces between the particles. This stabilization method is suitable in dilute systems of aqueous or polar organic media. The electric double layer is very unstable. It will easily be destroyed when there is a change in the concentration of the electrolyte and then result in particle agglomeration (Chow and Gonsalves, 1996; Orr, 1998).

The second method of stabilization involves steric forces. Surfactant molecules can adsorb onto the surfaces of particles and their lyophilic chains will